

1                   **Assessing the Liquefaction Hazard in the Groningen Region of the**  
2                   **Netherlands due to Induced Seismicity: Limitations of Existing Procedures**  
3                   **and Development of a Groningen-Specific Framework**

4  
5                   R.A. Green<sup>1</sup>, J.J. Bommer<sup>2</sup>, A. Rodriguez-Marek<sup>3</sup>, B.W. Maurer<sup>4</sup>,  
6                   P.J. Stafford<sup>5</sup>, B. Edwards<sup>6</sup>, P.P. Kruiver<sup>7</sup>, G. de Langes<sup>8</sup>, and J. van Elk<sup>9</sup>

7  
8  
9                   **Abstract** The Groningen gas field is one of the largest in the world and has produced over 2000  
10 billion m<sup>3</sup> of natural gas since the start of production in 1963. The first earthquakes linked to gas  
11 production in the Groningen field occurred in 1991, with the largest event to date being **M** 3.6. As  
12 a result, the field operator is leading an effort to quantify the seismic hazard and risk resulting from  
13 the gas production operations, including the assessment of liquefaction hazard. However, due to  
14 the unique characteristics of both the seismic hazard and the geological subsurface, particularly  
15 the unconsolidated sediments, direct application of existing liquefaction evaluation procedures is  
16 deemed inappropriate in Groningen. Specifically, the depth-stress reduction factor ( $r_d$ ) and the  
17 Magnitude Scaling Factor (MSF) relationships inherent to existing variants of the simplified  
18 liquefaction evaluation procedure are considered unsuitable for use. Accordingly, efforts have first  
19 focused on developing a framework for evaluating the liquefaction potential of the region for  
20 magnitudes ranging from **M** 3.5 to 7.0. The limitations of existing liquefaction procedures for use  
21 in Groningen and the path being followed to overcome these shortcomings are presented in detail  
22 herein.

23  
24                   **Keywords** Liquefaction, liquefaction hazard, induced seismicity, Groningen gas field

25  
26  
<sup>1</sup>Professor, Dept. of Civil and Environmental Engineering, Virginia Tech, Blacksburg, VA, USA (email: rugreen@vt.edu)

<sup>2</sup>Senior Research Investigator, Department of Civil and Environmental Engineering, Imperial College London, London, UK

<sup>3</sup>Professor, Dept. of Civil and Environmental Engineering, Virginia Tech, Blacksburg, VA, USA

<sup>4</sup>Assistant Professor, Dept. of Civil and Environmental Engineering, University of Washington, Seattle, WA, USA

<sup>5</sup>Reader, Dept. of Civil and Environmental Engineering, Imperial College London, London, UK

<sup>6</sup>Senior Lecturer, School of Environmental Sciences, University of Liverpool, Liverpool, UK

<sup>7</sup>Senior Geophysicist, Deltares, Delft, the Netherlands

<sup>8</sup>Senior Engineering Geologist, Deltares, Delft, the Netherlands

<sup>9</sup>Development Lead Groningen Asset, Nederlandse Aardolie Maatschappij B.V., Assen, the Netherlands

## 27 **1 Introduction**

28

29 The Groningen gas field is located in the northeastern region of the Netherlands and is one of the  
30 largest in the world. It has produced over 2000 billion m<sup>3</sup> of natural gas since the start of production  
31 in 1963. The first earthquakes linked to gas production in the Groningen field occurred in 1991,  
32 although earthquakes were linked to production at other gas fields in the region since 1986. To  
33 date the largest induced earthquake due to production at the Groningen field is the 2012 moment  
34 magnitude (**M**) 3.6 Huizinge event, and the largest recorded peak ground acceleration (PGA) is  
35 0.11 g which was recorded during a more recent, smaller (local magnitude, **M<sub>L</sub>**, 3.4) event. In  
36 response to concerns about the induced earthquakes, the field operator Nederlandse Aardolie  
37 Maatschappij (NAM) is leading an effort to quantify the seismic hazard and risk resulting from  
38 the gas production operations (Bourne et al. 2015, van Elk et al. 2017). In view of the widespread  
39 deposits of saturated sands in the region, the risk due to earthquake-induced liquefaction is being  
40 evaluated as part of this effort. Although an almost negligible contributor to earthquake fatalities,  
41 liquefaction triggering is an important threat to the built environment and in particular to  
42 infrastructure and lifelines (e.g., Bird and Bommer 2004).

43

44 Central to the liquefaction hazard/risk assessment of the Groningen field is the stress-based  
45 “simplified” liquefaction evaluation procedure, which is the most widely used approach to evaluate  
46 liquefaction potential worldwide. While most of the recently proposed variants of this procedure  
47 yield similar results for scenarios that are well represented in the liquefaction case history  
48 databases (e.g., Green et al. 2014), their predictions deviate, sometimes significantly, for other  
49 scenarios (e.g., low magnitude events; very shallow and very deep liquefiable layers; high fines  
50 content soils; medium dense to dense soils). These deviations result partly because existing  
51 variants of the simplified procedure are semi-empirical, hence they are apt for replicating existing  
52 data but lack proper extrapolation power. The empirical elements of existing procedures are  
53 derived from data from tectonic earthquakes in active shallow-crustal tectonic regimes such as  
54 California, Japan, and New Zealand. These conditions are different from those that of the  
55 Groningen field. Moreover, the geologic profiles/soil deposits in Groningen differ significantly  
56 from those used to develop the empirical aspects of the simplified procedure. As a result, the  
57 suitability of existing variants of the simplified procedure for direct use to evaluate liquefaction in

58 Groningen is questionable. Accordingly, prior to assessing the liquefaction hazard in Groningen,  
59 efforts have first focused on developing a framework for performing the assessment. This actually  
60 required a step backwards to develop an “unbiased” liquefaction triggering procedure for tectonic  
61 earthquakes, due to biases in relationships inherent to existing variants of the simplified procedure  
62 (e.g., Boulanger and Idriss 2014).

63  
64 In the following sections, the shortcomings in current variants of the simplified procedures for use  
65 in Groningen are detailed. Then, the efforts to develop a new “unbiased” variant of the simplified  
66 liquefaction evaluation procedure are presented. An outline of how this procedure is being  
67 modified for use in Groningen is presented next, followed by a brief overview of how the  
68 liquefaction hazard of Groningen will be assessed.

69  
70 **2 Shortcoming in existing variants of the simplified liquefaction evaluation procedure for**  
71 **use in Groningen**

72  
73 **2.1 Overview of the simplified procedure**

74  
75 As mentioned in the Introduction, the stress-based simplified liquefaction evaluation procedure is  
76 central to the approach adopted to assess the liquefaction hazard in the Groningen region. The  
77 word “simplified” in the procedure’s title originated from the proposed use of a form of Newton’s  
78 Second Law to compute cyclic shear stress ( $\tau_c$ ) imposed at a given depth in the soil profile, in lieu  
79 of performing numerical site response analyses (Whitman 1971; Seed and Idriss 1971). Inherent  
80 to this approach to computing the seismic demand is a depth-stress reduction factor ( $r_d$ ) that  
81 accounts for the non-rigid response of the soil profile and a Magnitude Scaling Factor (MSF) that  
82 accounts for the effects of the shaking duration on liquefaction triggering. For historical reasons  
83 the duration of an **M** 7.5 earthquake is used as the reference for MSF.

84  
85 Case histories compiled from post-earthquake investigations were categorized as either  
86 “liquefaction” or “no liquefaction” based on whether evidence of liquefaction was or was not  
87 observed. The seismic demand (or normalized Cyclic Stress Ratio: CSR\*) for each of the case  
88 histories is plotted as a function of the corresponding normalized *in situ* test metric, e.g., Standard

89 Penetration Test (SPT):  $N_{1,60cs}$ ; Cone Penetration Test (CPT):  $q_{c1Ncs}$ ; or small strain shear-wave  
90 velocity ( $V_s$ ):  $V_{s1}$ . In this plot, the “liquefaction” and “no liquefaction” cases tend to lie in two  
91 different regions of the graph. The “boundary” separating these two sets of case histories is referred  
92 to as the Cyclic Resistance Ratio ( $CRR_{M7.5}$ ) and represents the capacity of the soil to resist  
93 liquefaction during an **M** 7.5 event. This boundary can be expressed as a function of the normalized  
94 *in situ* test metrics.

95  
96 Consistent with the conventional definition for factor of safety (FS), the FS against liquefaction  
97 ( $FS_{liq}$ ) is defined as the capacity of the soil to resist liquefaction divided by the seismic demand:  
98

$$FS_{liq} = \frac{CRR_{M7.5}}{CSR^*} \quad (1)$$

99  
100 The Dutch National Annex to the Eurocode for the seismic actions (i.e., NPR 9998 2017),  
101 recommends the use of the Idriss and Boulanger (2008) variant of the simplified liquefaction  
102 evaluation procedure, but allows other variants to be used if they are in line with the safety  
103 philosophy of the NPR 9998-2017. As a result, the Idriss and Boulanger (2008) variant and the  
104 updated variant (Boulanger and Idriss 2014) have been used in several liquefaction studies in  
105 Groningen, resulting in predictions of potentially catastrophic liquefaction effects that have severe  
106 implications for buildings and for infrastructure such as dikes.

107

## 108 **2.2 Depth-stress reduction factor: $r_d$**

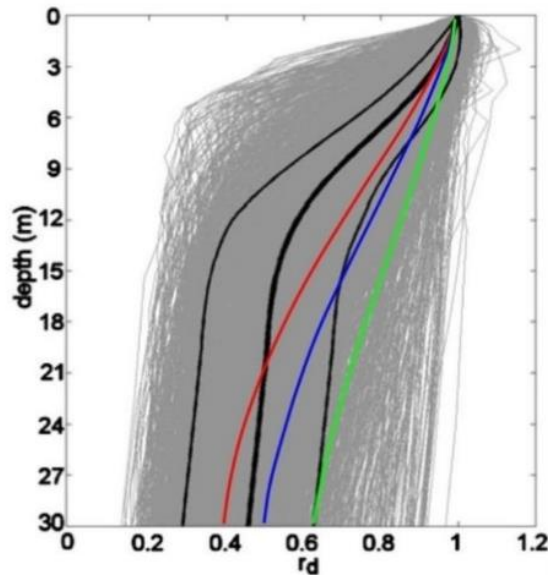
109

110 As stated above,  $r_d$  is an empirical factor that accounts for the non-rigid response of the soil profile.  
111 Both the Idriss and Boulanger (2008) and Boulanger and Idriss (2014) variants of the simplified  
112 liquefaction evaluation procedure use an  $r_d$  relationship that was developed by Idriss (1999). As  
113 shown in Figure 1, the Idriss (1999)  $r_d$  relationship is a function of earthquake magnitude and  
114 depth, with  $r_d$  being closer to one for larger magnitude events (note that  $r_d = 1$  for all depths  
115 corresponds to the rigid response of the profile). This is because larger magnitude events have  
116 longer characteristic periods and, hence, ground motions with longer wave lengths. As a result,  
117 even a soft profile will tend to respond as a rigid body if the characteristic wave length of the  
118 ground motions is significantly longer than the overall thickness of the profile. Accordingly, the

119 correlation between earthquake magnitude and the frequency content of the earthquake motions  
120 significantly influences the  $r_d$  relationship. This raises questions regarding the appropriateness of  
121 the Idriss (1999) relationship, which was developed using motions recorded during tectonic events,  
122 for evaluating liquefaction potential in Groningen where the seismic hazard is dominated by  
123 induced earthquakes having magnitudes less than  $M$  5.

124  
125 Another issue with the Idriss (1999)  $r_d$  relationship is that it tends to predict overly high CSR\*  
126 values at depth in a soil profile for tectonic events. This bias is illustrated in Figure 1 and is  
127 pronounced for depths between ~3 to 20 m below the ground surface. As a result, when used to  
128 evaluate case histories to develop the  $CRR_{M7.5}$  curves that are central to the procedure, the biased  
129  $r_d$  relationship results in a biased positioning of the  $CRR_{M7.5}$  curve. The significance of this issue  
130 is mitigated to some extent when the same  $r_d$  relationship used to develop the  $CRR_{M7.5}$  curve is  
131 also used in forward analyses (i.e., the bias cancels out). However, this will not be the case if  
132 site/region-specific  $r_d$  relationships are developed and used in conjunction with a  $CRR_{M7.5}$  curve  
133 that was developed using a “biased”  $r_d$  relationship.

134



135  
136 **Fig. 1** The red, blue, and green lines were computed using the Idriss (1999)  $r_d$  relationship for  $M$   
137 5.5,  $M$  6.5, and  $M$  7.5 events, respectively. The grey lines were computed by Cetin (2000) from  
138 equivalent linear site response analyses performed using a matrix of 50 soil profiles and 40  
139 motions. The black lines are the median (thick line) and median plus/minus one standard deviation

140 (thinner lines) for the Cetin (2000) analyses.

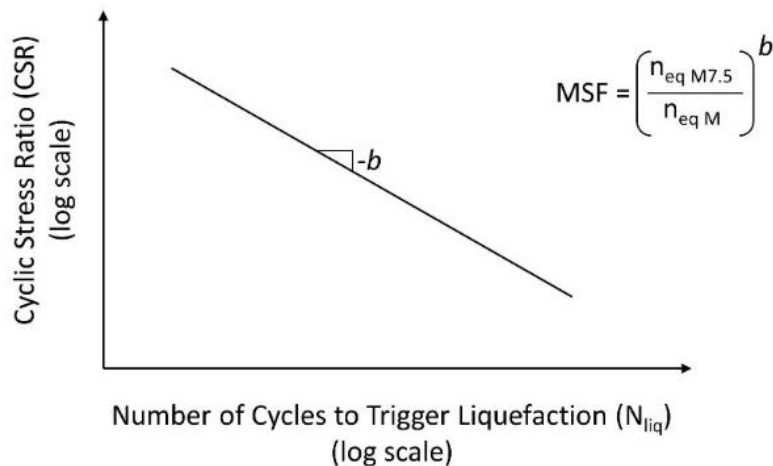
141

### 142 **2.3 Magnitude Scaling Factor: MSF**

143

144 As stated above, MSFs account for the influence of the strong motion duration on liquefaction  
145 triggering. MSFs have traditionally been computed as the ratio of the number of equivalent cycles  
146 for an **M** 7.5 event to that of a magnitude **M** event, raised to the power *b* [i.e.,  $MSF=(n_{eqM7.5}/n_{eqM})^b$ ].  
147 Both the Idriss and Boulanger (2008) and Boulanger and Idriss (2014) procedures used the Seed  
148 et al. (1975) variant of the Palmgren-Miner (P-M) fatigue theory to compute  $n_{eqM7.5}$  and  $n_{eqM}$  from  
149 earthquake motions recorded at the surface of soil profiles. Furthermore, they obtained the value  
150 of *b* from laboratory test data. The parameter *b* is the negative of the slope of a plot of log(CSR)  
151 versus log( $N_{liq}$ ), as shown in Figure 2;  $N_{liq}$  is the number of cycles required to trigger liquefaction  
152 in a soil specimen subjected to sinusoidal loading having an amplitude of CSR, typically  
153 determined using cyclic triaxial or cyclic simple shear tests.

154



155

156 **Fig. 2** Relationship between laboratory CSR vs.  $N_{liq}$  and MSF.

157

158 There are several shortcomings inherent to the approach used by Idriss and Boulanger (2008) and  
159 Boulanger and Idriss (2014) to compute the number of equivalent cycles and MSF. These include:

- 160 • Both the magnitude and uncertainty of  $n_{eq}$ , and hence MSF, are assumed to be constant with  
161 depth. However, Green and Terri (2005) have shown that  $n_{eq}$  can vary with depth in a given  
162 profile and Lasley et al. (2017) showed that while the median value for  $n_{eq}$  computed for a

163 large number of soil profiles and ground motions is relatively constant with depth, the  
164 uncertainty in  $n_{eq}$  varies with depth.

- 165 • Pulses in the acceleration time history having an amplitude less than  $0.3 \cdot a_{max}$  are assumed not  
166 to contribute to the triggering of liquefaction, and thus are not considered in the computation  
167 of  $n_{eq}$ . Using a relative amplitude criterion to exclude pulses is contrary to the known nonlinear  
168 response of soil which is governed by the absolute amplitude of the imposed load, among other  
169 factors. The use of a relative amplitude exclusion criterion with tectonic earthquake motions  
170 may inherently bias the resulting MSF.
- 171 • Each of the two horizontal components of ground motion is treated separately, inherently  
172 assuming that both components have similar characteristics. However, analysis of recorded  
173 motions has shown this is not always the case, particularly in the near fault region (e.g., Green  
174 et al. 2008; Carter et al. 2016). Groningen ground-motions recorded at short source-to-site  
175 distances often display pronounced polarization (Stafford et al. 2018).
- 176 • The  $b$  values used by Boulanger and Idriss (2014) were derived from several laboratory studies  
177 performed on various soils and it is uncertain whether all these studies used a consistent  
178 definition of liquefaction in interpreting the test data. As a result, the  $b$  values proposed by  
179 Boulanger and Idriss (2014) entail considerable uncertainty (Ulmer et al. 2018), with the  
180 proposed values not being in accord with those inherent to the shear modulus and damping  
181 degradation curves used in the equivalent linear site response analyses to develop the  $r_a$   
182 correlations (a point elaborated upon subsequently).
- 183 • Recent studies have shown that the residuals of the amplitude and duration of earthquake  
184 ground motions are negatively correlated (e.g., Bradley 2011) and this feature is clearly  
185 observed in the Groningen data (Bommer et al. 2016). None of the MSF correlations developed  
186 to date, to include the one proposed by Boulanger and Idriss (2014), have considered this.

187  
188 Some of the shortcomings listed above will be more significant to the Groningen liquefaction  
189 hazard assessment than others, but it is difficult to state *a priori* which ones these are. Furthermore,  
190 even for tectonic earthquakes the validation of MSF relationships is hindered by the limited  
191 magnitude range of case histories in the field liquefaction databases, with the majority of the cases  
192 being for events having magnitudes ranging from **M** 6.25 to **M** 7.75 (NRC 2016). Specific to the  
193 Groningen liquefaction hazard assessment, MSFs for small magnitude events are very important,

194 particularly given that published MSF relationships vary by a factor of 3 for  $M$  5.5 (Youd et al.  
195 2001), with this factor increasing if the proposed MSF relations are extrapolated to lower  
196 magnitudes.

197

### 198 **3 Removing bias from the simplified liquefaction evaluation procedure for tectonic** 199 **earthquakes**

200

#### 201 **3.1 Depth-stress reduction factor: $r_d$**

202

203 A new relationship for  $r_d$  was developed by Lasley et al. (2016) using an approach similar to that  
204 used by Cetin (2000). Equivalent linear site response analyses were performed on 50 soil profiles  
205 compiled by Cetin (2000) that are representative of those in the liquefaction case history databases.  
206 However, Lasley et al. (2016) used a larger set of recorded input motions in their analyses than  
207 were available at the time of the Cetin (2000) study. Several functional forms for  $r_d$  were examined  
208 by Lasley et al. (2016) in regressing the results from the site response analyses, with the following  
209 form selected because of its simplicity and fit of the data (i.e., relatively low standard deviation of  
210 the regressed data):

211

$$r_d = (1 - \alpha) \exp\left(\frac{-z}{\beta}\right) + \alpha + \varepsilon_{r_d} \quad (2a)$$

212

213 where  $z$  is depth in meters,  $\alpha$  is the limiting value of  $r_d$  at large depths and can range from 0 to 1,  
214 the variable  $\beta$  controls the curvature of the function at shallow depths, and  $\varepsilon_{r_d}$  is a zero-mean  
215 random variable with standard deviation  $\sigma_{r_d}$ . Expressions for  $\alpha$  and  $\beta$  are:

216

$$\alpha = \exp(-4.373 + 0.4491 \cdot M) \quad (2b)$$

$$\beta = -20.11 + 6.247 \cdot M \quad (2c)$$

217

218 and  $\sigma_{r_d}$  is defined as:

219

$$\sigma_{r_d} = \frac{0.1506}{[1 + \exp(-0.4975 \cdot z)]} \quad (2d)$$

220  
221 Relative to the other  $r_d$  relationships inherent to commonly used variants of the simplified  
222 procedure, the Lasley et al. (2016) model was developed using more site response data and more  
223 rigorous regression analyses. So while all relationships inherently have some bias, a strong  
224 argument can be made that Lasley et al. (2016) has the least bias of commonly used relationships  
225 and was therefore adopted for use herein.

226

### 227 **3.2 Magnitude Scaling Factor: MSF**

228

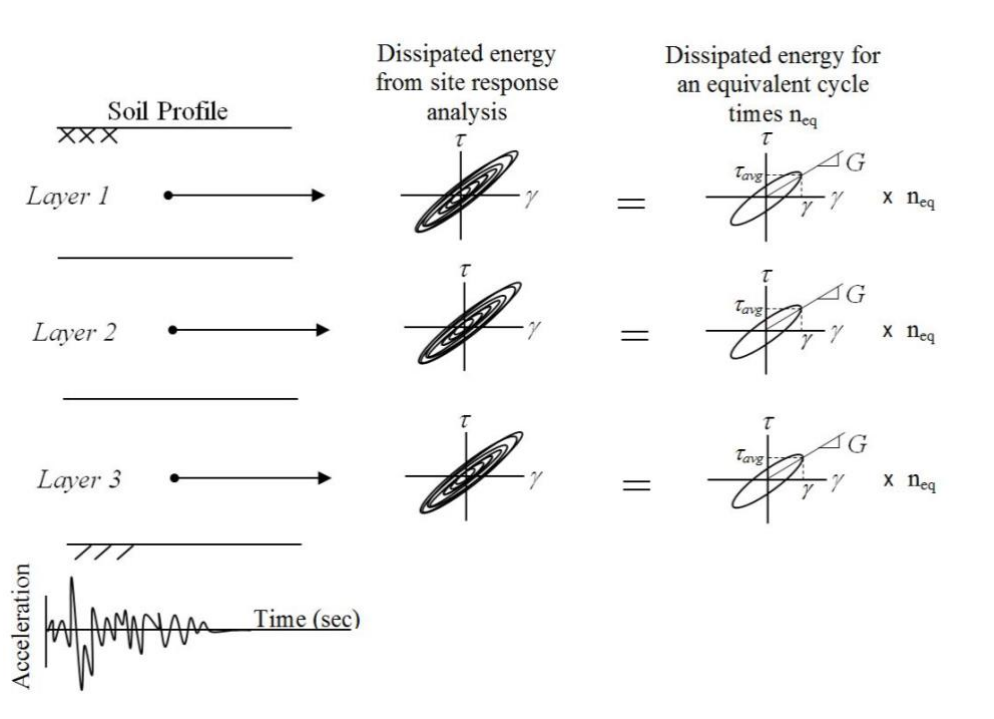
229 Development of a MSF relationship that overcomes all the shortcomings listed above for the Idriss  
230 and Boulanger (2008) and Boulanger and Idriss (2014) relationships is not as straightforward as  
231 developing the new  $r_d$  relationships. The reason for this is that there are many more issues with  
232 existing MSFs than there are with the  $r_d$  relationships. As a result, a new approach needed to be  
233 used to compute MSFs, as opposed to implementing an existing approach using a more  
234 comprehensive dataset and a more rigorous regression analysis.

235

236 As mentioned previously and shown in Figure 2, MSFs are computed from equivalent number of  
237 cycles,  $n_{eq}$ . Well-established fatigue theories have been proposed for computing  $n_{eq}$  for materials  
238 having varying phenomenological behaviour; reviews of different approaches for computing  $n_{eq}$   
239 are provided in Green and Terri (2005) and Hancock and Bommer (2005), among others.  
240 Developed specifically for use in evaluating liquefaction potential, the approach proposed by  
241 Green and Terri (2005) was selected for developing an  $n_{eq}$  relationship for the Groningen project.  
242 This approach is an alternative implementation of the P-M fatigue theory that better accounts for  
243 the nonlinear behaviour of the soil than the Seed et al. (1975) variant. In this approach, dissipated  
244 energy is explicitly used as the damage metric.  $n_{eq}$  is determined by equating the energy dissipated  
245 in a soil element subjected to an earthquake motion to the energy dissipated in the same soil  
246 element subjected to a sinusoidal motion of a given amplitude and a “duration” of  $n_{eq}$ . Dissipated  
247 energy was selected as the damage metric because it has been shown to correlate with excess pore  
248 pressure generation in saturated cohesionless soil samples subjected to undrained cyclic loading  
249 (e.g., Green et al. 2000; Polito et al. 2008). Furthermore, from a microscopic perspective, the  
250 energy is thought to be predominantly dissipated by the friction between sand grains as they move

251 relative to each other as the soil skeleton breaks down, which is requisite for liquefaction  
 252 triggering.

253  
 254 Conceptually, the Green and Terri (2005) approach for computing  $n_{eq}$  is shown in Figure 3. Stress  
 255 and strain time-histories at various depths in the soil profile are obtained from a site response  
 256 analysis. By integrating the variation of shear stress over shear strain, the cumulative dissipated  
 257 energy per unit volume of soil can be computed (i.e., the cumulative area bounded by the shear  
 258 stress-shear strain hysteresis loops).  $n_{eq}$  is then determined by dividing the cumulative dissipated  
 259 energy for the entire earthquake motion by the energy dissipated in one equivalent cycle. For  
 260 historical reasons, the shear stress amplitude of the equivalent cycle ( $\tau_{avg}$ ) is taken as  $0.65 \cdot \tau_{max}$   
 261 (where  $\tau_{max}$  is the maximum induced cyclic shear stress,  $\tau_c$ , at a given depth), and the dissipated  
 262 energy associated with the equivalent cycle is determined from the constitutive model used in the  
 263 site response analysis.



264  
 265 **Fig. 3** Illustration of the proposed procedure to compute  $n_{eq}$ . In this procedure, the energy  
 266 dissipated in a layer of soil, as computed from a site response analysis, is equated to the energy  
 267 dissipated in an equivalent cycle of loading multiplied by  $n_{eq}$ .

268  
 269 As noted above, one of the shortcomings of the Seed et al. (1975) variant of the P-M fatigue theory

270 is the way in which multi-directional shaking is taken into account. Specifically, each of the two  
 271 horizontal components of ground motion is treated separately, inherently assuming that both  
 272 components have similar characteristics. However, analysis of recorded motions has shown this is  
 273 not always the case, particularly in the near fault region (e.g., Green et al. 2008; Carter et al. 2016).  
 274 In contrast, Green and Terri (2005) accounted for multi-directional shaking by performing separate  
 275 site response analyses for each horizontal component in a pair of motions, adding the energy  
 276 dissipated at the respective depths for each component of motion, and setting the amplitude of the  
 277 equivalent cycle as 0.65 times the geometric mean of the maximum shear stresses experienced at  
 278 a given depth. This approach is referred to as “Approach 2” in Lasley et al. (2017) and is used  
 279 herein because it better accounts for differences in the characteristics in the two horizontal  
 280 components of motion.

281  
 282 Lasley et al. (2017) implemented the Green and Terri (2005) approach for computing  $n_{eq}$  using the  
 283 same motions and profiles used by Lasley et al. (2016) to develop their  $r_d$  relationship. Their  
 284 proposed  $n_{eq}$  relationship is:

$$\ln(n_{eq}) = 0.4605 - 0.4082 \cdot \ln\left(\frac{a_{max}}{g}\right) + 0.2332 \cdot M + \varepsilon_{Total} \quad (3a)$$

286  
 287 where  $a_{max}$  is in units of g and  $\varepsilon_{Total}$  is a zero-mean random variable with standard deviation  $\sigma_{Total}$   
 288 given by:

$$\sigma_{Total}(z) = \max\left[0.5399 - \frac{z}{26.4} (0.5399 - 0.4626), 0.4626\right] \quad (3b)$$

290  
 291  
 292 where  $z$  is depth in meters. The dependency of  $n_{eq}$  on  $a_{max}$  in Eq. 3 was chosen because of the  
 293 observed negative correlation of strong ground-motion duration with  $a_{max}$  (e.g., Bradley 2011).  
 294 Also, the functional form of this correlation is not an impediment to implementation because the  
 295 simplified liquefaction evaluation procedures require both the magnitude (for MSFs and  $r_d$ ) and  
 296  $a_{max}$  as input variables.

297

298 The  $b$  value that is needed to relate  $n_{eq}$  to MSFs (e.g., Figure 2) can also be determined from the  
299 constitutive model used in the site response analysis, by assuming that the CSR vs.  $N_{liq}$  curve  
300 shown in Figure 2 is a contour of constant dissipated energy (Figure 4). In Figure 4, the dissipated  
301 energy for a **M** 7.5 earthquake,  $\Delta W_{M7.5}$ , is computed using:

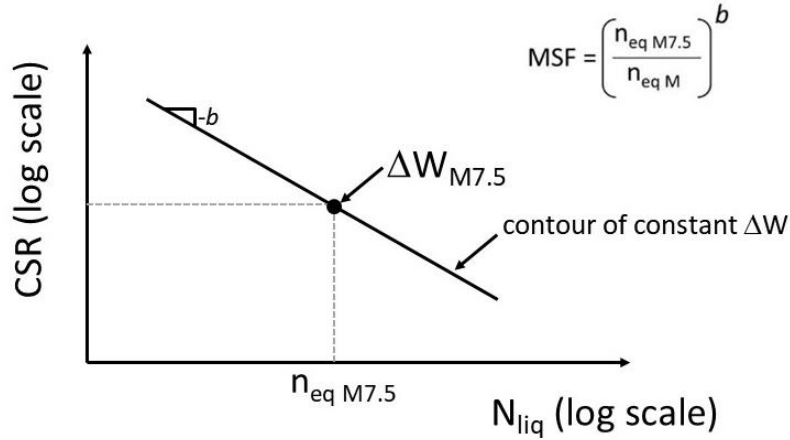
302

$$\Delta W_{M7.5} = \frac{2\pi \cdot D_{\gamma} \cdot \tau_c^2}{G_{max} \cdot \left(\frac{G}{G_{max}}\right)_{\gamma}} \cdot n_{eq\ M7.5} \quad (4)$$

303

304 where  $D_{\gamma}$  is the damping ratio for the induced shear strain  $\gamma$ ,  $\tau_c$  is the cyclic shear stress and  $G$  is  
305 the secant shear modulus. This equation is based on the assumption that the soil can be modelled  
306 as a visco-elastic material, consistent with the assumption inherent to the equivalent linear site  
307 response algorithm. For liquefaction evaluations,  $\tau_c$  used to compute  $\Delta W_{M7.5}$  can be determined  
308 from the  $CRR_{M7.5}$  curve from the simplified liquefaction evaluation procedure (e.g., Boulanger  
309 and Idriss 2014). Accordingly, the computed CSR vs.  $N_{liq}$  curve corresponds to a soil having a  
310 given  $q_{c1Ncs}$  and confined at an initial effective overburden stress ( $\sigma'_{vo}$ ) (i.e.,  $\tau_c = CRR_{M7.5} \times \sigma'_{vo}$ );  
311 the small strain shear modulus ( $G_{max}$ ) for the soil should be consistent with the penetration  
312 resistance used to determine  $CRR_{M7.5}$ . The damping ( $D_{\gamma}$ ) and the degraded secant shear modulus,  
313  $G_{max} \cdot (G/G_{max})_{\gamma}$ , values in Eq. (4) are commensurate with the induced shear strain ( $\gamma$ ) in the soil  
314 and can be determined iteratively from the shear modulus and damping degradation curves used  
315 to model the soil response (e.g., Darendeli and Stokoe 2001). Once the value of  $\Delta W_{M7.5}$  is  
316 determined, a contour of constant dissipated energy can be computed for different amplitudes of  
317 loading by simply computing the number of cycles for the assumed loading amplitude required for  
318 the dissipated energy to equal  $\Delta W_{M7.5}$ . The parameter  $b$  is assumed equal to the negative of the  
319 slope of the contour of constant dissipated energy. The assumption that the CSR vs.  $N_{liq}$  curve is a  
320 contour of constant dissipated energy inherently implies that the energy dissipated in a given  
321 element of soil at the point of liquefaction triggering is unique and independent of the imposed  
322 loading characteristics. Several studies have shown that this is a reasonable assumption (e.g.,  
323 Kokusho and Kaneko 2014; Polito et al. 2013).

324



325  
 326 **Fig. 4** A CSR vs.  $N_{liq}$  curve can be computed from shear modulus and damping degradation curves  
 327 assuming the curve is a contour of constant dissipated energy.  $\Delta W_{M7.5}$  can be computed using Eq.  
 328 (4) and the remaining portions of the curve can be computed for different amplitudes of loading  
 329 by simply computing the number of cycles for the assumed loading amplitude required for the  
 330 dissipated energy to equal  $\Delta W_{M7.5}$ .

331  
 332 The degradation curves proposed Darendeli and Stokoe (2001) were used herein to determine the  
 333  $b$  values following the procedure illustrated in Figure 4 for a range of effective confining stresses  
 334 and soil densities, with the resulting values ranging from 0.33 to 0.35. However,  $b = 0.34$  for the  
 335 vast majority of the confining stress-density combinations considered and was thus used herein to  
 336 compute MSFs from  $n_{eq}$ . Additionally,  $b = 0.34$  is consistent with laboratory curves developed  
 337 from high-quality undisturbed samples obtained by freezing (Yoshimi et al. 1984). Accordingly,  
 338 MSFs herein are computed as:

339

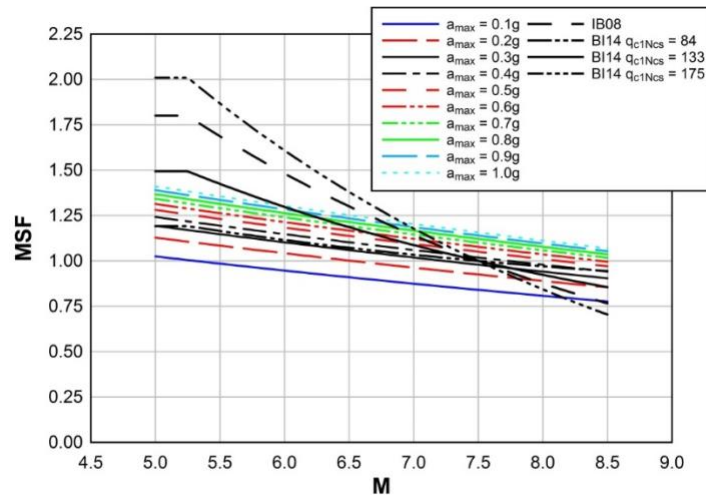
$$MSF = \left( \frac{n_{eq M7.5}}{n_{eq M}} \right)^b = \left( \frac{14}{n_{eq M}} \right)^{0.34} \leq 2.02 \quad (5a)$$

$$\sigma_{\ln(MSF)} = b \cdot \sigma_{\ln(n_{eq M})} = 0.34 \cdot \sigma_{\ln(n_{eq M})} \quad (5b)$$

340  
 341 where  $\sigma_{\ln(MSF)}$  is a first order approximation for the standard deviation of the natural log of the  
 342 MSF, and  $n_{eq M}$  and  $n_{eq M7.5}$  are computed using Eq. (3).

343  
 344 To compute  $n_{eq M7.5}$  using Eq. (3),  $\mathbf{M}$  is set to 7.5 and a corresponding value for  $a_{max}$  needs to be

345 assumed (i.e.,  $a_{max7.5}$ ). The value of  $a_{max7.5}$  was determined by computing the average  $a_{max}$  for the  
 346 case histories in the Boulanger and Idriss (2014) SPT and CPT liquefaction case history databases  
 347 ranging in magnitude from  $M$  7.4 to 7.6. The average  $a_{max}$  for the 116 case histories that fell within  
 348 this magnitude range was  $\sim 0.35$  g. Using this value for  $a_{max7.5}$ ,  $n_{eq M7.5}$  was computed to be  $\sim 14$ .  
 349 This value is similar to that determined by Seed et al. (1975), i.e.,  $n_{eq M7.5} = 15$ . However, the value  
 350 reported by Seed et al. (1975) represents the average for two horizontal components of motion,  
 351 while the value computed herein represents the combined influence of both components of motion  
 352 (Approach 2, Lasley et al. 2017). As a result, the value computed herein is approximately half of  
 353 that computed by Seed et al. (1975). This difference is due both to the significantly larger ground  
 354 motion database used by Lasley et al. (2017) to develop Eq. (3), where the motions used by Lasley  
 355 et al. (2017) represented a broader range of magnitudes and site-to-source distances compared to  
 356 those used by Seed et al. (1975), and to the differences in the approaches used to compute  $n_{eq}$ .  
 357 However, both of these differences also influence the denominator in Eq. (5a), which minimizes  
 358 their influence on the resulting MSF. The upper limit on the MSF (i.e., 2.02) corresponds to a  
 359 scenario where the earthquake motions consist of a single shear stress pulse in one of the horizontal  
 360 components of motion. A plot of Eq. (5a) is shown in Figure 5 for magnitudes ranging from  $M$  5.0  
 361 to 8.5 and  $a_{max}$  ranging from 0.1 to 1.0 g.



363  
 364 **Fig. 5** For a given magnitude earthquake, MSF developed herein increases as  $a_{max}$  increases. Also,  
 365 for comparison, the MSFs proposed by Idriss and Boulanger (2008) (IB08) and Boulanger and  
 366 Idriss (2014) (BI14) are also shown.

368 Figure 5 also shows a comparison of the MSF developed herein with those proposed by Idriss and  
 369 Boulanger (2008) and Boulanger and Idriss (2014), where the latter is shown for  $q_{c1Ncs} = 84, 133,$   
 370 and 175 atm. As may be observed from this figure, for a given value of  $a_{max}$  the MSF developed  
 371 herein has about the same dependency on magnitude as the MSF proposed by Boulanger and Idriss  
 372 (2014) for  $q_{c1Ncs} = 84$  atm (i.e., medium dense sand). However, the difference between the two is  
 373 that the former is a function of  $a_{max}$ , with MSF for a given magnitude increasing as  $a_{max}$  increases.

374

### 375 **3.3 “Unbiased” $CRR_{M7.5}$ curve**

376

377 The Lasley et al. (2016)  $r_d$  relationship and the MSF relationship developed herein were used to  
 378 reanalyse the CPT liquefaction case history database compiled by Boulanger and Idriss (2014); all  
 379 other parameters/relationships used to analyse the case history data were the same as those used  
 380 by Boulanger and Idriss (2014). These case histories were then used to regress a new “unbiased”  
 381 deterministic liquefaction triggering curve (i.e.,  $CRR_{M7.5}$  curve), which is shown in Figure 6. This  
 382 curve approximately corresponds to a probability of liquefaction [P(liq)] of 35% (total uncertainty)  
 383 and is given by:

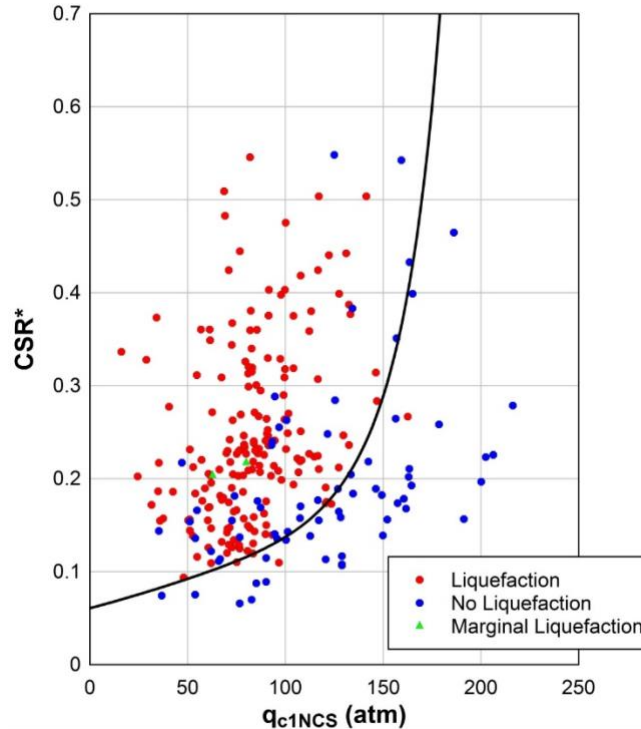
384

$$CRR_{M7.5} = exp \left\{ \left( \frac{q_{c1Ncs}}{113} \right) + \left( \frac{q_{c1Ncs}}{1000} \right)^2 - \left( \frac{q_{c1Ncs}}{140} \right)^3 + \left( \frac{q_{c1Ncs}}{137} \right)^4 - 2.8118706 \right\} \leq 0.6 \quad (6)$$

385

386 where  $q_{c1Ncs}$  is computed using the procedure outlined in Boulanger and Idriss (2014).

387



388

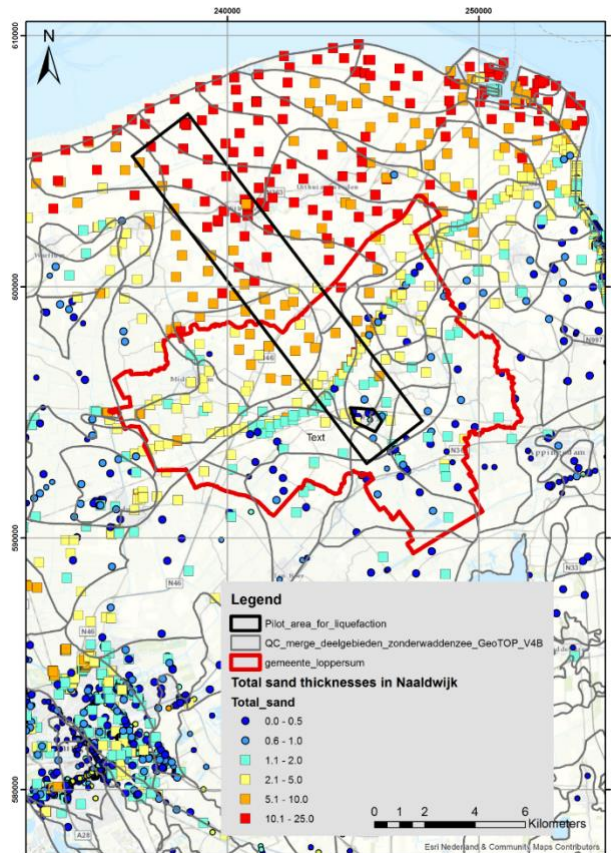
389 **Fig. 6** “Unbiased” deterministic CRR<sub>M7.5</sub> curve regressed from liquefaction case history data from  
 390 Boulanger and Idriss (2014) that were reanalysed using Lasley et al. (2016)  $r_d$  relationship and  
 391 MSF developed herein.

392

#### 393 **4 Assessment of liquefaction hazard in Groningen**

394

395 To determine whether a Groningen-wide liquefaction hazard assessment is warranted, a  
 396 liquefaction hazard pilot study is being performed first, wherein the study area was selected to  
 397 simultaneously satisfy three criteria: (a) proximity to the region of highest shaking hazard; (b)  
 398 sampling of areas with sand deposits that are thick, shallow, young, and loose; and (c) sampling  
 399 of multiple site-response zones used in developing the Groningen-specific ground-motion model  
 400 (Rodriguez-Marek et al. 2017). The location of the pilot study area is shown in Figure 7, along  
 401 with the cumulative thicknesses of the Holocene sand deposits that comprise the Naaldwijk  
 402 formation which is considered to have the highest liquefaction potential in the region (Korff et al.  
 403 2017). However, before the liquefaction pilot study can be performed, Groningen-specific  $r_d$  and  
 404 MSF relationships must be developed following the approaches used by Lasley et al. (2016, 2017)  
 405 and presented above. The soil/geologic profiles and ground motions used to develop the  
 406 Groningen-specific relationships are detailed below.



408

409 **Fig. 7** Location of the liquefaction pilot study area across the Groningen gas field. Also shown are  
 410 the cumulative thicknesses of the Holocene sand deposits that comprise the Naaldwijk formation.

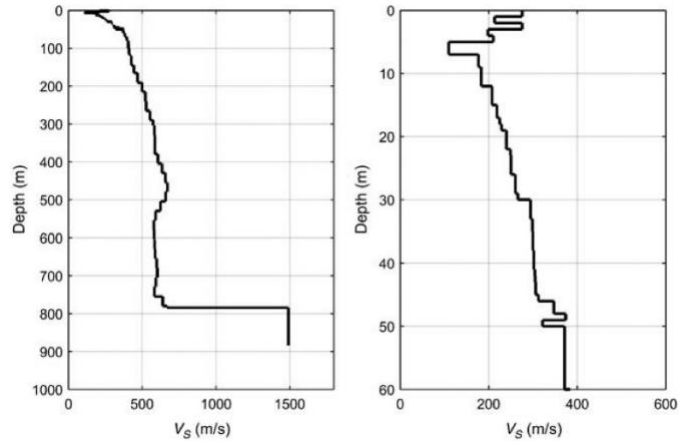
411

#### 412 **4.1 Groningen-specific $r_a$ and MSF relationships**

413

414 The geological setting of Groningen, including detailed cross sections, is described in Kruiver et  
 415 al. (2017a), and the velocity model from the selected reference rock horizon (at ~ 800 m depth) to  
 416 the ground surface is described in detail by Kruiver et al. (2017b). An example of the resulting  $V_s$   
 417 profiles is shown in Figure 8. The unit weights of the strata in the profiles are also needed for the  
 418 site response analyses. Towards this end, the assignment of unit weight is based on representative  
 419 values for stratigraphic lithological units derived from CPTs using Lunne et al. (1997). For some  
 420 of the deeper formations, the density is assumed to be constant, consistent with the borehole logs  
 421 from two deep boreholes (Kruiver et al., 2017a, b).

422



423  
 424 **Fig. 8** Sample Vs profile at the location of one of the many ground-motion recording stations in  
 425 the field. The plot on the left is the full profile down to reference rock horizon (depth of ~800 m),  
 426 and the plot on the right is an enlarged view of the upper 60 m of the profile. (Rodriguez-Marek et  
 427 al. 2017)

428  
 429 The software SMSIM (Boore 2005, version 16/12/2009) was used in conjunction with the  
 430 Groningen-specific model parameters to generate motions at the reference horizon (Bommer et al.  
 431 2017) for magnitudes ranging from **M** 3.5 to 7.0 and epicentral distances ranging from 0.1 to 60  
 432 km. The lower bound was chosen on the basis of no liquefaction having been observed in the field  
 433 to date and to explore the full range of potential triggering events, despite the fact that globally  
 434 there is no reliable evidence of liquefaction triggering by earthquakes smaller than **M** 4.5 (Green  
 435 and Bommer 2018). The upper value in the maximum magnitude distribution is **M** 7.25 as  
 436 determined by an expert panel (Bommer and van Elk 2017).

437  
 438 Once developed, the Groningen-specific  $r_d$  and MSF relationships can be used in conjunction with  
 439 the  $CRR_{M7.5}$  curve shown in Figure 6 to compute the  $FS_{liq}$  at depth in profiles in Groningen  
 440 subjected to induced earthquake motions. The computation of liquefaction hazard curves that will  
 441 be used to determine whether the hazard due to liquefaction is significant enough to require the  
 442 consequences from liquefaction to be assessed is discussed next.

443  
 444  
 445  
 446

## 4.2 Planned output from the liquefaction hazard study

The liquefaction hazard will be calculated using a Monte Carlo method (Bourne et al. 2015) wherein probability distributions for activity rates (Bourne and Oates 2017), event locations and magnitudes, and resulting ground motions will be sampled such that the simulated future seismic hazard is consistent with historical seismic and reservoir compaction datasets. For each event scenario, the developed Groningen-specific relationships will be used to compute the  $FS_{liq}$  as a function of depth for ~100 profiles across the pilot study area.

The “Ishihara inspired LPI” ( $LPI_{ish}$ ) framework will be used to relate computed  $FS_{liq}$  to the predicted the severity of surficial liquefaction manifestation, which has been shown to correlate to liquefaction damage potential for level ground sites. The  $LPI_{ish}$  framework was proposed by (Maurer et al. 2015a) and is a conceptual and mathematical merger of the Ishihara (1985)  $H_1$ - $H_2$  chart and Liquefaction Potential Index (LPI) framework (Iwasaki et al. 1978). The most notable differences between the original LPI and  $LPI_{ish}$  frameworks are that the latter better accounts for the influence of the non-liquefiable crust on the severity of surficial liquefaction manifestations (Green et al. 2018) and more appropriately weights the contribution of shallower liquefied layers to surficial manifestations (van Ballegooy et al. 2014). The  $LPI_{ish}$  framework was chosen for this study because it has been shown to yield more accurate predictions of the severity of surficial liquefaction manifestations than competing indices (Maurer et al. 2015a, b): LPI (Iwasaki et al. 1978) and LSN (van Ballegooy et al. 2014).

The output from the liquefaction pilot study will be liquefaction hazard curves for the ~100 sites in the study area, where the hazard curves show the annual frequency of exceedance (AFE) of varying  $LPI_{ish}$  values for a site. Consistent with the requirements of NPR 9998-2017 (NPR 9998 2017), which was specifically for the Groningen field,  $LPI_{ish}$  values corresponding to an AFE of  $\sim 4 \times 10^{-4}$  (or a 2475-year return period) will be of interest. The results from this pilot study will differ from previous liquefaction studies performed for Groningen, where liquefaction was evaluated in previous studies for earthquake scenarios (i.e., ground motions and magnitudes) corresponding to a given return period (i.e., a “pseudo-probabilistic” approach).

478 The optimal  $LPI_{ish}$  thresholds corresponding to different severities of surficial liquefaction  
479 manifestations are dependent on the liquefaction triggering procedure used to compute  $FS_{liq}$  and  
480 the characteristics of the profile. However, without liquefaction case history data to develop  
481 Groningen-specific thresholds, the thresholds proposed by Iwasaki et al. (1978) will be  
482 conservatively (Maurer et al. 2015c) used in the pilot study with the  $LPI_{ish}$  framework (i.e.,  $LPI_{ish}$   
483  $< 5$ : none to minor surficial liquefaction manifestations are predicted;  $LPI_{ish} > 15$ : severe surficial  
484 liquefaction manifestations are predicted).

485

## 486 **5 Discussion and conclusions**

487

488 The presence of saturated loose deposits of young sands in the Groningen field region creates the  
489 necessity to assess the potential for liquefaction triggering by the earthquakes being induced by  
490 the gas production as an integral component of the seismic risk analysis. The application of  
491 liquefaction hazard assessment procedures calibrated for larger-magnitude tectonic earthquakes in  
492 other regions has resulted in predictions of potentially catastrophic liquefaction effects, with severe  
493 implications for buildings and for infrastructure such as dikes. Despite the fact these estimates,  
494 sometimes associated with earthquake scenarios only fractionally greater than the lower bound for  
495 events that have been observed globally to trigger liquefaction that poses a threat to the built  
496 environment (Green and Bommer 2018), the dissemination of such results has raised great concern  
497 regarding liquefaction hazard in Groningen.

498

499 Due to the unique characteristics of both the seismic hazard and the geologic profiles/soil deposits  
500 in Groningen, direct application of existing variants of the simplified liquefaction evaluation  
501 procedure is deemed inappropriate for assessing the liquefaction hazard of the region, including  
502 the Idriss and Boulanger (2008) procedure recommended in the NPR 9998-2017 and the updated  
503 variant, Boulanger and Idriss (2014). Accordingly, efforts were first focused on re-analyzing the  
504 liquefaction case histories that were compiled for natural earthquakes to remove bias in their  
505 interpretation. Towards this end, new a depth-stress reduction factor ( $r_d$ ) and number of equivalent  
506 cycles ( $n_{eq}$ )/magnitude scaling factor (MSF) relationships for shallow crustal active tectonic  
507 regimes were developed and used in the reanalysis of the cone penetration test (CPT)  
508 “liquefaction” and “no liquefaction” case histories compiled by Boulanger and Idriss (2014). These

509 case histories were then used to regress a new “unbiased” deterministic liquefaction triggering  
510 curve (or cyclic resistance ratio curve:  $CRR_{M7.5}$ ). The “unbiased” procedure can be readily adapted  
511 to evaluate liquefaction potential in regions with unique profiles and/or ground motions, such as  
512 Groningen. This is being achieved by using similar approaches to those employed to develop the  
513 new  $r_d$  and MSF relationships for tectonic earthquakes (Lasley et al. 2016, 2017) to develop  
514 Groningen-specific relationships using motions and soil profiles characteristic to Groningen.

515  
516 The liquefaction hazard will be calculated using a Monte Carlo method wherein probability  
517 distributions for activity rates, event locations and magnitudes, and resulting ground motions are  
518 sampled such that the simulated future seismic hazard is consistent with historical seismic and  
519 reservoir compaction datasets for events having magnitudes ranging from  $M$  3.5 to 7.0. For each  
520 event scenario, the Groningen-specific relationships will be used to compute the factor of safety  
521 ( $FS_{liq}$ ) against liquefaction as a function of depth for ~100 profiles across the liquefaction pilot  
522 study area and corresponding Ishihara inspired Liquefaction Potential Index ( $LPI_{ish}$ ) (Maurer et al.  
523 2015a) hazard curves are being computed for each profile. The hazard curves specify the return  
524 periods of different severities of surficial liquefaction manifestations, with the severities  
525 corresponding to a return period of 2475 years being of interest per the NPR 9998-2017. This is in  
526 marked contrast to previous liquefaction hazard studies performed for Groningen that used a  
527 pseudo-probabilistic approach, where the  $FS_{liq}$  or LPI is computed for an earthquake scenario (i.e.,  
528 ground motions and magnitude) corresponding to a given return period.

529  
530 The framework of the liquefaction hazard pilot study is in complete accord with the safety  
531 philosophy of the NPR 9998-2017 and is particularly well suited to the specific nature of the time-  
532 dependent induced seismicity being considered. The results of the study will form the basis on  
533 which decisions will be made regarding the need for implementing mitigation measures. The  
534 liquefaction hazard study is benefiting significantly from the broader efforts to assess the regional  
535 seismic hazard in Groningen, to include the development of a regional velocity model (Kruiver et  
536 al. 2017a, b), site response model (Rodriguez-Marek et al. 2017), and ground-motion prediction  
537 model (Bommer et al. 2017).

538  
539

540 **Acknowledgments**

541  
542 This research was partially funded by National Science Foundation (NSF) grants CMMI-1030564  
543 and CMMI-1435494 and Nederlandse Aardolie Maatschappij B.V. (NAM). This support is  
544 gratefully acknowledged. This study has also significantly benefited from enlightening discussions  
545 with colleagues at Shell, Deltares, Arup, Fugro, Beca, and on the NEN liquefaction task force.  
546 However, any opinions, findings, and conclusions or recommendations expressed in this material  
547 are those of the authors and do not necessarily reflect the views of the NSF or NAM.

548

549 **References**

550

551 Bird JF, Bommer JJ (2004) Earthquake losses due to ground failure. *Engineering Geology*  
552 75(2):147-179.

553

554 Bommer JJ, van Elk J (2017) Comment on ‘The maximum possible and the maximum expected  
555 earthquake magnitude for production-induced earthquakes at the gas field in Groningen, the  
556 Netherlands’ by Gert Zöller and Matthias Holschneider. *Bulletin of the Seismological Society of*  
557 *America* 107(3):1564-1567.

558

559 Bommer JJ, Dost B, Edwards B, Stafford PJ, van Elk J, Doornhof D, Ntinalexis M (2016)  
560 Developing an Application-Specific Ground-Motion Model for Induced Seismicity. *Bulletin of the*  
561 *Seismological Society of America* 106(1):158–173.

562

563 Bommer JJ, Stafford PJ, Edwards B, Dost B, v. Dedem E, Rodriguez-Marek A, Kruiver P, van Elk  
564 J, Doornhof D, Ntinalexis M (2017) Framework for a ground-motion model for induced seismic  
565 hazard and risk analysis in the Groningen gas field, the Netherlands. *Earthquake Spectra*  
566 33(2):481-498.

567

568 Boore DM (2005) SMSIM – Fortran programs for simulating ground motions from earthquakes:  
569 Version 2.3 – A Revision of OFR 96-80, USGS Open-File Report 00-509, U.S. Geological Survey,  
570 Reston VA.

571  
572 Boulanger RW, Idriss IM (2014) CPT and SPT Based Liquefaction Triggering Procedures. Report  
573 No. UCD/CGM-14/01, University of California at Davis, Davis, CA.  
574  
575 Bourne SJ, Oates SJ (2017) Extreme threshold failures within a heterogeneous elastic thin-sheet  
576 account for the spatial-temporal development of induced seismicity within the Groningen gas field.  
577 Journal of Geophysical Research: Solid Earth 122. DOI: 10.1002/2017JB014356.  
578  
579 Bourne SJ, Oates SJ, Bommer JJ, Dost B, van Elk J, Doornhof D (2015) A Monte Carlo method  
580 for probabilistic seismic hazard assessment of induced seismicity due to conventional gas  
581 production. Bulletin of the Seismological Society of America 105:1721–1738.  
582  
583 Bradley BA (2011) Correlation of significant duration with amplitude and cumulative intensity  
584 measures and its use in ground motion selection. Journal of Earthquake Engineering 15:809–832.  
585  
586 Carter WL, Green RA, Bradley BA, Wotherspoon LM, Cubrinovski M (2016) Spatial Variation  
587 of Magnitude Scaling Factors During the 2010 Darfield and 2011 Christchurch, New Zealand,  
588 Earthquakes. Soil Dynamics and Earthquake Engineering 91:175-186.  
589  
590 Cetin KO (2000) Reliability-based assessment of seismic soil liquefaction initiation hazard. Ph.D.  
591 Thesis, University of California at Berkeley, Berkeley, CA.  
592  
593 Darendeli MB, Stokoe II KH (2001) Development of a new family of normalized modulus  
594 reduction and material damping curves. Geotechnical Engineering Report GD01-1, University of  
595 Texas at Austin, Austin, TX.  
596  
597 Green RA, Bommer JJ (2018) What is the smallest earthquake magnitude that can trigger  
598 liquefaction? Earthquake Spectra (*in review*).  
599  
600 Green RA, Terri GA (2005) Number of equivalent cycles concept for liquefaction evaluations -  
601 revisited. Journal of Geotechnical and Geoenvironmental Engineering 131(4):477-488.

602  
603 Green RA, Mitchell JK, Polito CP (2000). An energy-based excess pore pressure generation model  
604 for cohesionless soils. Proceedings of The John Booker Memorial Symposium – Developments in  
605 Theoretical Geomechanics (D.W. Smith and J.P. Carter, eds.), A.A. Balkema, Rotterdam, The  
606 Neatherlands, 383-390.  
607  
608 Green RA, Lee J, White TM, Baker JW (2008) The significance of near-fault effects on  
609 liquefaction. Proc. 14<sup>th</sup> World Conf. on Earthquake Engineering, Paper No. S26-019.  
610  
611 Green RA, Cubrinovski M, Cox B, Wood C, Wotherspoon L, Bradley B, Maurer B (2014) Select  
612 liquefaction case histories from the 2010-2011 Canterbury earthquake sequence. Earthquake  
613 Spectra 30:131-153.  
614  
615 Green RA, Maurer BW, van Ballegooy S (2018) The influence of the non-liquefied crust on the  
616 severity of surficial liquefaction manifestations: Case history from the 2016 Valentine’s Day  
617 earthquake in New Zealand. Proc. Geotechnical Earthquake Engineering and Soil Dynamics V  
618 (GEESD V), Austin, TX, 10-13 June. (*in press*)  
619  
620 Hancock J, Bommer JJ (2005) The effective number of cycles of earthquake ground motion.  
621 Earthquake Engineering and Structural Dynamics 34:637-664.  
622  
623 Idriss IM (1999) An update to the Seed-Idriss simplified procedure for evaluating liquefaction  
624 potential. Proc., TRB Workshop on New Approaches to Liquefaction, Publication No. FHWA-  
625 RD-99- 165, Federal Highway Administration.  
626  
627 Idriss IM, Boulanger RW (2008) Soil liquefaction during earthquakes. Monograph MNO-12,  
628 Earthquake Engineering Research Institute, Oakland, CA, 261 pp.  
629  
630 Ishihara K (1985) Stability of natural deposits during earthquakes. Proc. 11<sup>th</sup> Intern. Conf. on Soil  
631 Mechanics and Foundation Engineering, San Francisco, CA, USA, 1:321-376.  
632

633 Iwasaki T, Tatsuoka F, Tokida K, Yasuda S (1978) A practical method for assessing soil  
634 liquefaction potential based on case studies at various sites in Japan. Proc. 2<sup>nd</sup> Intern. Conf. on  
635 Microzonation, Nov 26-Dec 1, San Francisco, CA, USA.

636  
637 Kokusho T, Kaneko Y (2014) Dissipated & strain energies in undrained cyclic loading tests for  
638 liquefaction potential evaluations. Proc. Tenth US National Conf. on Earthquake Engineering, July  
639 21-25, 2014, Anchorage, Alaska, DOI: 10.4231/D3DR2P89D

640  
641 Korff M, Wiersma A, Meijers P, Kloosterman F, de Lange G, van Elk J, Doornhof D (2017)  
642 Liquefaction mapping for induced seismicity based on geological and geotechnical features. Proc.  
643 3<sup>rd</sup> Intern. Conf. on Performance-Based Design in Earthquake Geotechnical Engineering (PBDIII),  
644 Vancouver, Canada, 16-19 July, 2017.

645  
646 Kruiver PP, Wiersma A, Kloosterman FH, de Lange G, Korff M, Stafleu J, Busscher F, Harting  
647 R, Gunnink JL, Green RA, van Elk J, Doornhof D (2017a). Characterisation of the Groningen  
648 subsurface for seismic hazard and risk modelling. Netherlands Journal of Geosciences 96(5):s215-  
649 s233.

650  
651 Kruiver PP, van Dedem E, Romijn R, de Lange G, Korff M, Stafleu J, Gunnink JL, Rodriguez-  
652 Marek A, Bommer JJ, van Elk J, Doornhof D (2017b) An integrated shear-wave velocity model  
653 for the Groningen gas field, The Netherlands, Bulletin of Earthquake Engineering. doi:  
654 10.1007/s10518-017-0105-y.

655  
656 Lasley S, Green RA, Rodriguez-Marek A (2016). A new stress reduction coefficient relationship  
657 for liquefaction triggering analyses. Technical Note, Journal of Geotechnical and  
658 Geoenvironmental Engineering 142(11):06016013-1.

659  
660 Lasley S, Green RA, Rodriguez-Marek A (2017) Number of equivalent stress cycles for  
661 liquefaction evaluations in active tectonic and stable continental regimes. Journal of Geotechnical  
662 and Geoenvironmental Engineering 143(4):04016116-1.

663

664 Lunne T, Robertson PK, Powell JJM (1997) Cone Penetration Testing in Geotechnical Practice,  
665 EF Spon/Blackie Academic, Routledge Publishers, London, United Kingdom, 312 pp.  
666

667 Maurer BW, Green RA, Taylor, O-DS (2015a) Moving towards an improved index for assessing  
668 liquefaction hazard: Lessons from historical data. *Soils and Foundations* 55(4):778-787.  
669

670 Maurer BW, Green RA, Cubrinovski M, Bradley BA (2015b) Calibrating the Liquefaction  
671 Severity Number (LSN) for competing liquefaction evaluation procedures: A case study in  
672 Christchurch, New Zealand. Proc. 6<sup>th</sup> Intern. Conf. on Earthquake Geotechnical Engineering  
673 (6ICEGE), Christchurch, New Zealand, 2-4 November.  
674

675 Maurer BW, Green RA, Cubrinovski M, Bradley BA (2015c) Fines-Content Effects on  
676 Liquefaction Hazard Evaluation for Infrastructure in Christchurch, New Zealand. *Soil Dynamics  
677 and Earthquake Engineering* 76:58-68.  
678

679 NPR 9998 (2017) Assessment of structural safety of buildings in case of erection, reconstruction  
680 and disapproval – Basis rules for seismic actions: induced earthquakes. NEN, Delft, Netherlands.  
681

682 National Research Council (NRC) (2016) State of the Art and Practice in the Assessment of  
683 Earthquake-Induced Soil Liquefaction and Consequences. Committee on Earthquake Induced Soil  
684 Liquefaction Assessment, National Research Council, The National Academies Press,  
685 Washington, DC.  
686

687 Polito CP, Green RA, Lee J (2008) Pore pressure generation models for sands and silty soils  
688 subjected to cyclic loading. *Journal of Geotechnical and Geoenvironmental Engineering*  
689 134(10):1490-1500.  
690

691 Polito C, Green RA, Dillon E, Sohn C (2013) The effect of load shape on the relationship between  
692 dissipated energy and residual excess pore pressure generation in cyclic triaxial tests. *Canadian  
693 Geotechnical Journal* 50(9):1118-1128.  
694

695 Rodriguez-Marek A, Kruiver PP, Meijers P, Bommer JJ, Dost B, van Elk J, Doornhof D (2017) A  
696 regional site-response model for the Groningen gas field. Bulletin of the Seismological Society of  
697 America 107(5):2067-2077.  
698

699 Seed HB, Idriss IM (1971) Simplified procedure for evaluating soil liquefaction potential. Journal  
700 of the Soil Mechanics and Foundations Division 97(SM9):1249–273.  
701

702 Seed HB, Idriss IM, Makdisi F, Banerjee N (1975) Representation of irregular stress time histories  
703 by equivalent uniform stress series in liquefaction analysis. Report Number EERC 75-29,  
704 Earthquake Engineering Research Center, College of Engineering, University of California at  
705 Berkeley, Berkeley, CA.  
706

707 Stafford PJ, Zurek BD, Ntinalexis M, Bommer JJ (2018) Extensions to the Groningen ground-  
708 motion model for seismic risk calculations: Component-to-component variability and spatial  
709 correlation. This volume.  
710

711 Ulmer KJ, Upadhyaya S, Green RA, Rodriguez-Marek A, Stafford PJ, Bommer JJ, van Elk J  
712 (2018) A Critique of b-values Used for Computing Magnitude Scaling Factors. Proc. Geotechnical  
713 Earthquake Engineering and Soil Dynamics V (GEESD V), Austin, TX, 10-13 June. (*in press*)  
714

715 van Ballegooy S, Malan P, Lacrosse V, Jacka ME, Cubrinovski M, Bray JD, O'Rourke TD,  
716 Crawford SA, Cowan H (2014) Assessment of liquefaction-induced land damage for residential  
717 Christchurch. Earthquake Spectra 30(1):31-55.  
718

719 van Elk J, Doornhof D, Bommer JJ, Bourne SJ, Oates SJ, Pinho R, Crowley H (2017) Hazard and  
720 risk assessments for induced seismicity in Groningen. Netherlands Journal of Geoscience  
721 96(5):s259-s269.  
722

723 Whitman RV (1971) Resistance of soil to liquefaction and settlement. Soils and Foundations  
724 11(4):59-68.  
725

726 Yoshimi Y, Tokimatsu K, Kaneko O, Makihara Y (1984). Undrained cyclic shear strength of dense  
727 Niigata sand. *Soils and Foundations*, 24(4):131-145.  
728  
729 Youd TL, Idriss IM, Andrus RD, Arango I, Castro G, Christian JT, Dobry R, Finn WDL, et al.  
730 (2001) Liquefaction Resistance of Soils: Summary Report from the 1996 NCEER and 1998  
731 NCEER/NSF Workshops on Evaluation of Liquefaction Resistance of Soils. *Journal of*  
732 *Geotechnical and Geoenvironmental Engineering* 127(4):297-313.